Probing the Function, Conformational Plasticity, and Dimer−Dimer Contacts of the GluR2 Ligand-Binding Core: Studies of 5-Substituted Willardiines and GluR2 S1S2 in the Crystal[†,‡]

Rongsheng Jin[§] and Eric Gouaux*[,§,||]

Department of Biochemistry and Molecular Biophysics and Howard Hughes Medical Institute, Columbia University, New York, New York 10032

Received October 22, 2002; Revised Manuscript Received February 4, 2003

ABSTRACT: Numerous naturally occurring and synthetic α-amino acids act as agonists on (*S*)-2-amino-3-(3-hydroxy-5-methyl-4-isoxazole) propionic acid (AMPA) receptors but nevertheless display significant differences in their functional properties and modes of interaction. The 5-substituted willardiines are a series of compounds that exhibit a range of affinities, act as partial agonists, and give rise to intermediate levels of activation and desensitization. However, the molecular basis for the activities of 5-substituted willardiines has not been conclusively elaborated at the level of atomic resolution. Here we provide insight into the molecular basis of the potency and efficacy elicited by the 5-substituted willardiines on the basis of cocrystal structures with the GluR2 ligand-binding core. We also show that the crystallized ligand-binding core has an affinity for agonists similar to the ligand-binding core in solution. Analysis of multiple crystal lattices suggests modes by which the ligand-binding core dimers interact in the tetrameric receptor. These studies further our understanding of how subtle differences in the structures of agonists are correlated to changes in the conformation of residues and water molecules in the immediate binding pocket and to the degree of domain closure.

Ionotropic glutamate receptors (iGluRs)[1] are ligand-gated ion channels that are best known for their roles in fast excitatory synaptic transmission in the mammalian nervous system (*1*, *2*). iGluRs are essential to the development and homeostasis of the nervous system and are implicated in a number of disease and injury states such as schizophrenia and stroke (*3*−*6*). Perhaps surprisingly, iGluR antagonists inhibit the growth of colon adenocarcinoma, astrocytoma, breast and lung carcinoma cells (*7*, *8*), and malignant glioma cells (*9*). Even though iGluRs are activated by the ubiquitous neurotransmitter L-glutamate, there are substantial differences in the pharmacological profiles of different receptors; thus, the family of glutamate receptors has been subdivided according to agonist specificity (*10*).

iGluR agonist specificity accurately foreshadowed the segregation of receptor subtypes on the basis of amino acid sequence, and (*S*)-2-amino-3-(3-hydroxy-5-methyl-4-isoxazole) propionic acid (AMPA), kainate, and *N*-methyl-D-aspartate (NMDA) receptors do indeed form distinct receptor subfamilies (*11*−*14*). While most of the divergence in amino acid sequence is remote from the agonist-binding cleft, there are a number of amino acid differences in and around the binding cleft that play a significant role in the determination of agonist specificity. Mirroring the diversity of iGluR amino acid sequences, there are a great number of compounds that bind to the glutamate site and display a range of potency (affinity), efficacy (activation), and receptor subtype specificity (*10*). To understand the determinants of agonist potency, efficacy, and specificity, we have carried out crystallographic and physiological studies of the GluR2 receptor with a series of 5-substituted willardiines (*15*, *16*).

Full agonists of AMPA receptors produce maximum peak current or efficacy and profound desensitization, while partial agonists induce submaximum responses, incomplete desensitization, and exhibit a ∼10^3-fold range of potency. Although the previously determined structures of the GluR2 ligand-binding core have provided insights into the action of receptor antagonists and agonists (*17*−*22*), important questions related to the action of partial agonists, to the functional state of the ligand-binding core in crystals, and to the arrangement of the ligand-binding cores in the intact receptor remain unanswered.

To facilitate structural and functional studies on iGluRs, we have developed the GluR2 S1S2J construct (*23*) that encapsulates the ligand-binding core and is suitable for high-

[†] This work was supported by the National Alliance for Research on Schizophrenia and Depression and the NIH. E.G. is a Klingenstein Research Fellow and an assistant investigator with the Howard Hughes Medical Institute.

[‡] The coordinates for the crystal structures described here have been deposited with the Protein Data Bank (see Supporting Information).

* To whom correspondence should be addressed. E-mail: jeg52@columbia.edu. Phone: (212) 305-4475. Fax: (212) 305-8174.

[§] Department of Biochemistry and Molecular Biophysics.

[||] Howard Hughes Medical Institute.

[1] Abbreviations: iGluRs, ionotropic glutamate receptors; GluR2, ionotropic glutamate receptor subtype 2 or B; AMPA, (*S*)-2-amino-3-(3-hydroxy-5-methyl-4-isoxazole) propionic acid; NMDA, *N*-methyl-D-aspartate; S1S2J, J construct of the genetically engineered GluR2 ligand-binding core; HW, willardiine; FW, 5-fluorowillardiine; BrW, 5-bromowillardiine; IW, 5-iodowillardiine; PEG, poly(ethylene glycol); ASU, asymmetric unit; TEVC, two-electrode voltage clamp; EC_{50}, concentration where agonist elicits 50% maximum current response in a TEVC experiment; IC_{50}, concentration of agonist that displaces 50% of the bound radioactivity in a ligand-binding experiment.

10.1021/bi020632t CCC: $25.00
Published on Web 04/18/2003

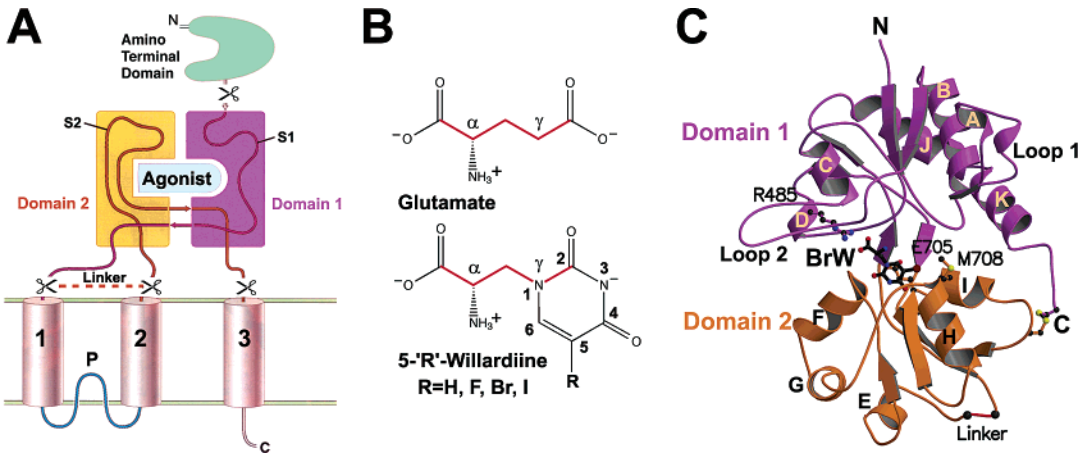

FIGURE 1: (A) Domain structure of iGluRs. The two domains of the ligand-binding core (S1S2) are colored in purple and yellow, while the amino-terminal domain (ATD) is in green. Scissors indicate the locations that are modified to generate the ligand-binding core. (B) Chemical structures of glutamate and 5-substituted willardiines. (C) Ribbon representation of the structure of GluR2 ligand-binding core in complex with BrW. Domains 1 and 2 are purple and orange, respectively. BrW, key binding site residues R485, E705, M708, the amino (N) and carboxyl (C) termini, and helices A−K are labeled. The C718−C773 disulfide bond is drawn and is located at the carboxyl terminus of S2.

resolution structural analysis, as shown in Figure 1 (*17*, *18*, *24*−*26*). On the basis of structural, biophysical, and physiological experiments on the isolated ligand-binding core and the full-length receptor, we suggest that the binding of agonist and the subsequent closure of the cleft in the ligand-binding core are coupled to channel activation and to desensitization. The studies of Sun and co-workers (*27*) focused on how changes in the strength of the dimer interface affect the extent of receptor desensitization when the receptor is activated by full agonists such as glutamate. While the strength of the dimer interface is an important factor in governing the desensitization of the receptor in the context of a full agonist, it is not clear why different partial agonists, acting on the same receptor, should elicit different degrees of receptor desensitization. Because the 5-substituted series of halogenated willardiine compounds only differ by the identity of a single atom and because substitution at the 5-position yields compounds that have a range of potency, efficacy, and receptor subtype specificity (*15*, *16*), the willardiines provide a subtle vehicle by which to probe the relationships between structure and function in the GluR2 receptor.

To assay the functional behavior of the GluR2 S1S2 ligand-binding core in crystals, we carried out a novel titration experiment in which we demonstrated that the affinity of the S1S2J fragment for ligand in crystals is similar to that for the identical fragment in solution, thus indicating that the lattice interactions do not significantly affect the functional behavior of the S1S2J ligand-binding core. We have also taken advantage of the multiple crystal forms produced during the course of these investigations to determine modes by which the ligand-binding core dimers interact in crystals, and using these results, suggest a plausible arrangement for the ligand-binding core dimers in the intact receptor.

EXPERIMENTAL PROCEDURES

Materials. The 5-substituted willardiine compounds were obtained from Tocris, were all of the (*S*) stereoisomer, were used without further purification, and were dissolved in aqueous solution with 1.1 M equiv. of sodium hydroxide. The GluR2 S1S2J construct has been described previously (*18*).

Protein Preparation. Protein expression, refolding, and purification, in the presence of glutamate, were performed as previously described (*25*, *26*, *28*). The sequence of the rat GluR2 S1S2J (flop) construct used in this study begins with $GAN_{392}K$, where the native GluR2 sequence begins with Asn 392. The numbering of the polypeptide begins with the predicted first residue of the mature receptor and does not include the signal peptide. Prior to crystallization, glutamate was removed from the S1S2J protein by dialyzing extensively against a buffer composed of 10 mM HEPES, pH 7.0, 20 mM NaCl, and 1 mM EDTA, and the protein was concentrated to ~10 mg/mL (calculated ϵ_{280} is 39,640 M^{-1} cm^{-1}).

Crystallization and Data Collection. The ligand concentrations used for cocrystallization were 5 mM for 5-fluorowillardiine (FW), 10 mM for willardiine (HW), 10 mM for 5-bromowillardiine (BrW), and 10 mM for 5-iodowillardiine (IW). Crystals were grown at 4 °C by hanging drop vapor diffusion, and drops contained a 1:1 ratio of protein and reservoir solution. BrW and IW complexes were separately crystallized in two different crystal forms. One common crystal form is the AMPA/glutamate-like crystal form, referred to here as the zinc form (Zn form) (*18*). All other forms described will be referred to as non-zinc forms (non-Zn form). The crystallization conditions of HW, FW, BrW (non-Zn form), and IW (non-Zn form) have been published (*29*). Reservoir solutions for the Zn form crystals were as follows: BrW, 12−16% PEG 8000, 0.25−0.3 M ammonium sulfate, 0.05 M zinc acetate, and 0.1 M sodium cacodylate, pH 6.5; IW, 10−15% PEG 4000, 0.25−0.3 M ammonium sulfate, 0.1−0.16 M zinc acetate, and 0.1 M Tris-HCl, pH 7.5.

All diffraction data were collected at 110 K. Crystals were soaked in the corresponding crystallization buffer supplemented with ligand and 12−16% glycerol before flash cooling in liquid nitrogen. Data for the Zn form BrW and IW complexes were collected at beamline X4A, National Synchrotron Light Source, Brookhaven National Laboratory. All diffraction data sets were processed with the HKL suite of programs (*30*). The Zn form BrW and IW cocrystals belong to the $P2_12_12$ space group, have similar unit cell dimensions, and are isomorphous to the AMPA/glutamate crystal form (*18*).

Table 1: Data Collection Statistics

ligand	space group	unit cell dimension (Å)	# per A.U.[a]	λ (Å)	d_{min}[b] (Å)	mean redundancy	R_{merge}[c,d] (%)	completeness[d] (%)
BrW−Zn	$P2_12_12$	$a = 114.06$, $b = 163.41$, $c = 47.85$	3	0.9879	1.75(1.81)	5.76	5.1(17.4)	94.4(70.5)
IW−Zn	$P2_12_12$	$a = 113.84$, $b = 163.80$, $c = 48.01$	3	0.9879	1.90(2.02)	4.60	5.3(28.2)	95.2(79.2)

[a] Number of protein molecules per asymmetric unit (A.U.). [b] Values in parentheses define the low resolution limits for the last shell of data. [c] $R_{merge} = (\sum|I_i - \langle I_i\rangle|)/\sum_I|I_i|$, where $\langle I_i\rangle$ is the mean I_i over all symmetry-equivalent reflections. [d] Values in parentheses indicate statistics for the last shell of data.

Table 2: Refinement Statistics

										rms deviations			
							average B value			bonds	angles	B values	
ligand	res. (Å)	R_{work}[a] (%)	R_{free}[b] (%)	# protein atoms	# water	# ligand atoms	overall	main chain	ligand	(Å)	(deg)	bonds	angles
BrW−Zn	30−1.75	21.1	25.5	5886	646	45	21.33	19.36	17.79	0.010	1.479	1.942	2.860
IW−Zn	30−1.90	21.3	26.2	5831	474	45	24.84	23.02	22.43	0.010	1.489	2.452	3.545

[a] $R_{work} = (\sum||F_o| - |F_c||)/\sum|F_o|$, where F_o and F_c denote observed and calculated structure factors, respectively. [b] Five percent of the reflections were set aside for the calculation of the R_{free} value.

Structure Determination and Analysis. The structures of the Zn form BrW and IW complexes were solved by difference Fourier using the isomorphous Zn form AMPA structure as an initial model (*18*). Relevant crystallographic statistics are presented in Tables 1 and 2. All structure refinements were performed with X-PLOR or CNS (*31*, *32*), and the program O was used for model building (*33*). Refinements were begun with rigid body minimization followed by a slow-cool, simulated-annealing protocol at 5000 K to reduce model bias. Iterative rounds of positional and individual temperature factor refinement were performed in conjunction with model building into omit maps until the R_{free} converged (*34*). The ligands were not included until the R_{free} was below 0.32. Least squares superpositions were calculated using LSQMAN (*35*), and the extent of domain closure was determined using the program FIT (*36*) and was defined as the rotation required to fit domain 2 following superposition of domain 1, using α-carbon atoms in the superpositions. MOLSCRIPT (*37*), BOBSCRIPT (*38*), and Raster3D (*39*) were used to make figures.

Ligand Displacement Experiments in the Crystal. Crystals for soaking experiments were grown using a reservoir solution consisting of 15−17% PEG 8000, 0.12−0.19 M zinc acetate, 0.1 M sodium cacodylate, pH 6.5, and 2 mM AMPA. These crystals were also the reference AMPA cocrystals. For the AMPA displacement experiments, the soaking solutions were the same as the original AMPA cocrystal reservoir solution except that 350 nM AMPA and BrW (10 nM to 10 mM) were included. Soaking was carried out at 4 °C, in sitting drops using microbridges, and crystals were transferred to the soaking solutions using cryo-loops. Crystals were soaked in 30 μL of solution, and they were washed three times with 30 μL of fresh soaking solution with each change of solution. The soakings at seven different BrW concentrations (10 nM, 100 nM, 1 μM, 10 μM, 100 μM, 1 mM, and 10 mM) were carried out at the same time, and the crystals were handled in a comparable way. The soaking solution was changed every 24−48 hrs for a total of 12 times. The crystals were flash frozen in liquid nitrogen 19 days after the first soaking, and X-ray data collection was carried out over the following 3 days.

Ligand Displacement Experiments in Solution. Purified GluR2-S1S2J protein was dialyzed extensively against ligand binding buffer (30 mM Tris-HCl, pH 7.2, 100 mM potassium thiocyanate, 2.5 mM calcium chloride, and 10% glycerol) prior to binding experiments (*24*, *25*). For competition binding studies, 350 nM ^{3}H-AMPA (10.6 Ci/mmol) was incubated with various concentrations of BrW (1 nM to 10 mM). GSWP 02500 membranes were used for filter binding. Nonspecific binding was determined in the presence of 1 mM glutamate. Ligand-binding experiments were carried out in duplicate, and results are the average of the two experiments.

Data Collection and Structure Determination for Soaked Crystals. Glycerol (16% v/v) was used as the cryo protectant for all crystals. Selection of the energy for data collection (0.91843 Å, bromine K edge) was based on a fluorescence scan of BrW cocrystals. The single wavelength anomalous data sets were collected on a Quantum 4 CCD detector using inverse beam geometry. The HKL suite of programs was used for data processing. The structures were solved by difference Fourier using either the AMPA or the BrW Zn form structures as models. The refinements were carried out with CNS and begun with separate positional refinements using either an AMPA or a BrW structure model (without ligand) as the starting structure. The structure that gave the lower crystallographic *R* factor was chosen for further refinement. Water molecules and zinc ions in the AMPA or BrW structures were included in subsequent positional and temperature factor refinements. Refinements were continued until the crystallographic R_{free} value converged. The anomalous difference maps were calculated using the CCP4 program suite when the anomalous difference amplitude was used, and the phase angle was retarded by 90°. The maps were inspected in O. The anomalous signals of bromine atoms or zinc ions were defined as the peak height in anomalous difference Fourier maps. The domain closure was determined using the program FIT.

RESULTS

Displacement of AMPA by BrW in the Crystal. To test the extent to which studies in crystals are related to functional studies of the receptor in solution, we designed a series of crystal titration experiments. The titration experiments began with the Zn form AMPA cocrystals grown in the presence

Table 3: Crystallographic Statistics for Soaking Experiments

BrW concentration[a]	unit cell dimension (Å)	d_{min}[b] (Å)	mean redundancy	R_{merge}[c,d] (%)	completeness[d] (%)	R_{work}[e] (%)	R_{free}[f] (%)
AMPA	$a = 114.54$, $b = 164.10$, $c = 47.40$	1.80(1.86)	3.0	6.9(16.6)	91.4(61.2)	22.5	24.4
10 nM	$a = 114.40$, $b = 164.55$, $c = 47.36$	1.90(1.97)	3.5	5.5(13.3)	93.6(74.3)	21.2	24.8
100 nM	$a = 114.48$, $b = 164.20$, $c = 47.40$	1.90(1.97)	4.2	5.6(12.6)	98.4(93.1)	22.6	24.9
1 μM	$a = 114.42$, $b = 163.58$, $c = 47.25$	1.90(1.97)	4.4	6.1(13.1)	96.5(84.6)	22.8	25.6
10 μM	$a = 114.75$, $b = 164.01$, $c = 47.82$	1.90(1.97)	3.6	6.0(20.2)	92.2(75.8)	22.6	25.9
100 μM	$a = 114.53$, $b = 163.76$, $c = 48.04$	2.00(2.07)	4.1	7.0(20.3)	98.3(94.4)	21.4	25.0
1 mM	$a = 114.35$, $b = 163.68$, $c = 48.02$	1.85(1.92)	4.0	5.0(27.4)	90.7(57.4)	22.5	25.2
10 mM	$a = 114.49$, $b = 163.28$, $c = 47.96$	1.95(2.02)	3.9	6.3(26.3)	90.3(89.0)	20.8	24.8
BrW	$a = 114.29$, $b = 163.40$, $c = 48.07$	1.80(1.86)	4.5	6.1(20.3)	90.2(55.2)	21.1	23.4

[a] Crystals grown in the presence of 2 mM AMPA or 10 mM BrW were used as control. For soaking experiments, crystals were originally grown with 2 mM AMPA and soaked in different concentrations of BrW together with 350 nM AMPA. [b] Values in parentheses define the low resolution limits for the last shell of data. [c] $R_{merge} = (\sum|I_i - \langle I_i\rangle|)/\sum_i|I_i|$, where $\langle I_i\rangle$ is the mean I_i over all symmetry-equivalent reflections. [d] Values in parentheses indicate statistics for the last shell of data. [e] $R_{work} = (\sum||F_o| - |F_c||)/\sum|F_o|$, where F_o and F_c denote observed and calculated structure factors, respectively. [f] Ten percent of the reflections were set aside for the calculation of the R_{free} value.

of 2 mM AMPA. Two or three AMPA cocrystals were then soaked in 30 μL of mother liquor solution supplemented with 350 nM AMPA, which is about 15-fold above the K_d value in solution (*18*), and concentrations of BrW ranging from 10 nM to 10 mM. With each solution change, the crystals were washed 2−3 times with fresh soaking solution, thus enhancing the exchange of interstitial solution with the fresh soaking solution and ensuring that the concentration of free ligand was approximately equal to total ligand concentration. Additional experiments in which X-ray diffraction data sets were collected and analyzed at intermediate time points showed that the soaking protocol was sufficient to equilibrate the crystal with the soaking solution.

Structures representing each of the data points in the crystal titration experiments were solved by difference Fourier using either the AMPA or the BrW structure as a starting model (Table 3). Exhaustive refinements, using only a single structure in each refinement, were carried out for all data sets. The diffraction data obtained from crystals titrated with low BrW concentrations gave lower crystallographic *R* values when using the AMPA structure as an initial model, while the data from soakings at high BrW concentrations yielded lower *R* values when using the BrW structure as an initial model, suggesting that there is a transition between the AMPA-like and the BrW-like complex structure in going from low to high BrW concentrations.

Superposition of the refined structures with either domain 1 or domain 2 gave lower root-mean-square deviations (rmsd) in comparison with superposition using both domains, indicating that the two domains behaved like rigid bodies and that the most significant conformational changes were due to the clam shell movement of the two domains. Of the three protomers in the asymmetric unit (A, B, C), protomer C in the Zn form was chosen for further analysis because it participates in the fewest zinc-mediated interprotomer interactions. Accordingly, the mean temperature factor for protomer C (28.58 Å^2) is higher than those for protomer A (22.78 Å^2) and protomer B (21.26 Å^2) in all the structures solved in the titration experiments.

Using protomer C of the cocrystallized AMPA complex as a reference, the domain closure of the structures solved at different BrW concentrations was examined. This analysis shows that intermediate concentrations of BrW lead to different degrees of domain closure that are intermediate between the fully closed AMPA conformation and the partially open BrW conformation. In Figure 3A, we see that the changes of domain closure show a typical binding curve yielding an EC_{50} value of 6.8 μM. At the intermediate concentration of 10 μM BrW, refinement using a single model yielded a degree of domain closure approximately halfway between the AMPA-like and the BrW-like conformations. Because we thought that this might be due to multiple conformations of the ligand-binding core in the crystal, we carried out another simulated annealing refinement protocol using two entire and independent molecules. However, this resulted in neither a lower R_{free} nor a significant difference in conformation of the two independent protein molecules. Therefore, we would suggest that at 10 μM BrW, the crystal lattice stabilizes a conformation of the ligand binding core that has an intermediate degree of domain closure, even though approximately 50% of the molecules are bound with AMPA and 50% with BrW.

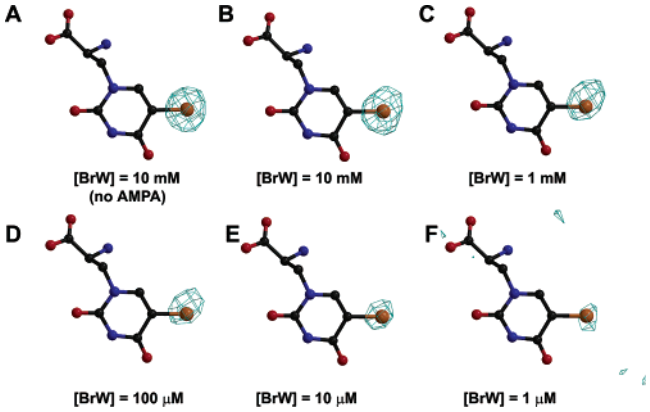

FIGURE 2: Anomalous difference Fourier maps calculated using data from crystals that were soaked in solutions with varying concentrations of BrW, using protomer C as an example. The maps were contoured at 10σ in panels A−E and at 3.5σ in panel F. (A) Difference density calculated using data from a reference crystal grown in the presence of 10 mM BrW; (B−F) difference density from crystals soaked in a range of concentrations of BrW (10 mM to 1 μM) together with 350 nM AMPA. There were no peaks in maps calculated using data from crystals that were soaked in 100 nM and 10 nM BrW.

In addition to the conformational changes of the clam shell, we can also monitor the displacement of AMPA by BrW by taking advantage of the anomalous scattering from the bromine atom (Figure 2). The anomalous scattering of the zinc ions in the crystal lattice provides an internal reference,

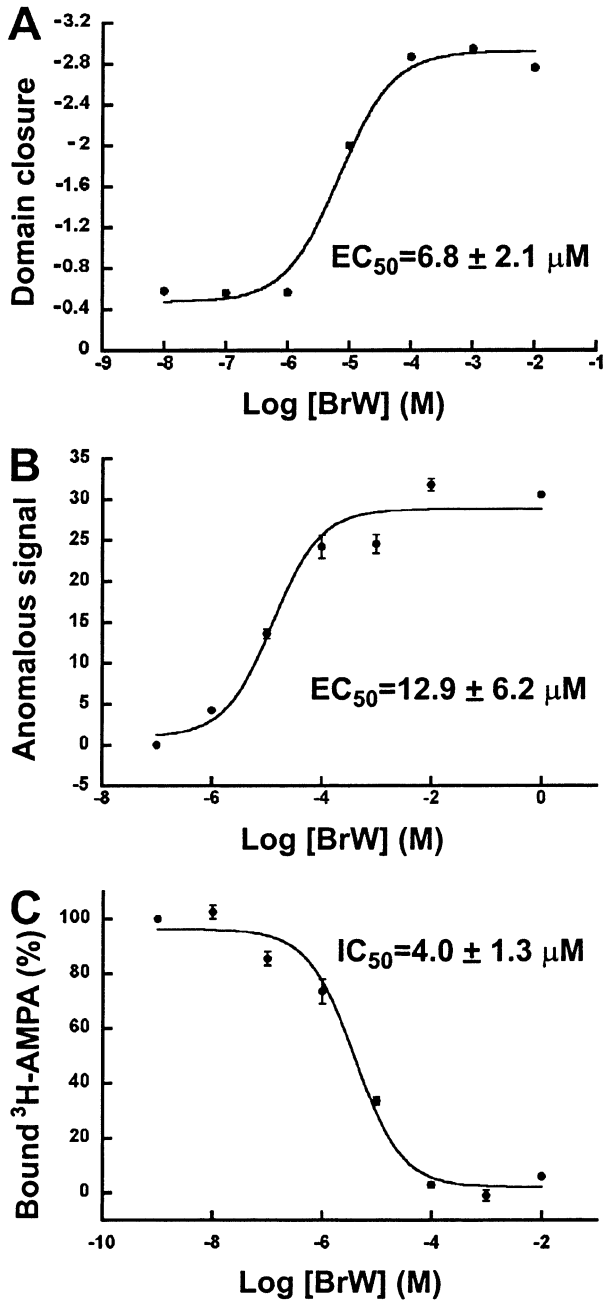

FIGURE 3: Crystal titration studies demonstrate that, even in the crystal lattice, the GluR2 ligand-binding core can undergo conformational changes that are linked to ligand binding. (A) Using molecule C of the AMPA complex as a reference, the changes in domain closure because of the soaking of AMPA cocrystals in various concentrations of BrW are plotted against the corresponding BrW concentrations. (B) The electron density from the bromine anomalous diffraction is plotted against the corresponding BrW concentrations. In both panels A and B, molecule C of the zinc form is used for comparisons. (C) Competition binding of BrW against 350 nM ^{3}H-AMPA in solution, as described in Experimental Procedures.

making it possible to compare the anomalous signals of the bromine atoms from different soaking experiments. Using the BrW cocrystal structure as a reference, the anomalous signals of the BrW bromine atoms from different crystals were scaled to a similar level so that the anomalous signals of the corresponding zinc ions were the same in all structures. The scaling was done separately according to the five different zinc atoms in the asymmetric unit. The means and standard errors were then calculated based on the scaled results derived from each of the five zinc ions and plotted against the corresponding BrW concentration. The analysis from the BrW site in protomer C yielded an EC_{50} value of 12.9 μM (Figure 3B). In a competition experiment carried out in solution using 350 nM ^{3}H-AMPA, we obtained an IC_{50} value of 4.0 μM for BrW (Figure 3C).

Willardiines Bind Similarly in Comparison to Glutamate. The structures of GluR2 S1S2J with three full agonists and five partial agonists have been solved in this lab, providing us with a unique opportunity to compare the ligand binding modes of the GluR2 receptor (*17*, *18*, *22*). When the α-carbon atoms from domain 1 are superimposed, we see that there is conservation in the binding of the α-amino and α-carboxyl groups, but the substituents attached to the γ-position occupy different positions, as shown in Figure 4 for FW and IW. To classify the binding subsites, we have extended the terminology of Armstrong and Gouaux (*18*) and have defined nine positions (A−E, F1−2, G, and H) within the binding pocket that are common interaction sites for AMPA receptor agonists (Figure 5). All α-carboxyl and α-amino groups occupy the highly conserved subsites A and B (*18*), forming five and two direct interactions with domain 1 and domain 2, respectively. The γ-substituents of the willardiines faithfully mimic the γ-carboxyl group of glutamate and occupy the subsites D and E. However, the isoxazole ring of AMPA binds in subsite E while recruiting a water molecule for site D. Interestingly, the willardiines promote conformational changes in subsite D, and the distance between the 2-carbonyl oxygen of the willardiines and the OH of Thr 655 is ∼3.1 Å, while the equivalent distance is ∼3.3 Å in the full agonist structures; the estimated error in the coordinates is between 0.2 and 0.3 Å on the basis of a Luzzati plot. In addition, the distances between the 2-carbonyl oxygen of willardiines and the NH of Ser 654 are 3.3 and 3.5 Å for BrW and IW complexes, respectively, while they are less than 3.2 Å in the HW, FW, kainate, and full agonist glutamate, AMPA, and quisqualate complexes.

Subsite F Distinguishes Full and Partial Agonists. Subsite F is occupied by either an agonist atom or a water molecule, and in the glutamate complex, for example, water W4 occupies subsite F. Structural comparisons suggest that binding at this position can be further divided into two subsites, F1 and F2, helping to differentiate full and partial agonists. Subsite F1 represents the binding site for full agonists, occupied by the 2-nitrogen atom in the isoxazole ring of AMPA (*18*), the 5-carbonyl oxygen in the oxadiazolidine ring of quisqualate (*22*), and water W4 in the glutamate structure (*18*). The F2 subsite, which is occupied by the 4-carbonyl oxygen of the willardiines and a water molecule in the kainate complex (*17*, *18*), is located ∼1.4 Å away from F1 site and is farther from domain 1 (Figure 5). However, both F1 and F2 subsites interact with Glu 705 and water W3, the latter of which forms hydrogen bonds with Thr 686 and Tyr 702 (Figure 4).

The conserved water molecules in the binding pocket play critical roles in mediating ligand−protein interactions. Water W2 bridges residues Leu 650/Leu 703 and full agonist atoms positioned at site E. Because of the more open cleft conformation in the willardiine complexes, W2 moves farther away from domain 1, relative to its position in full agonist complexes. Although maintaining its interactions with Leu

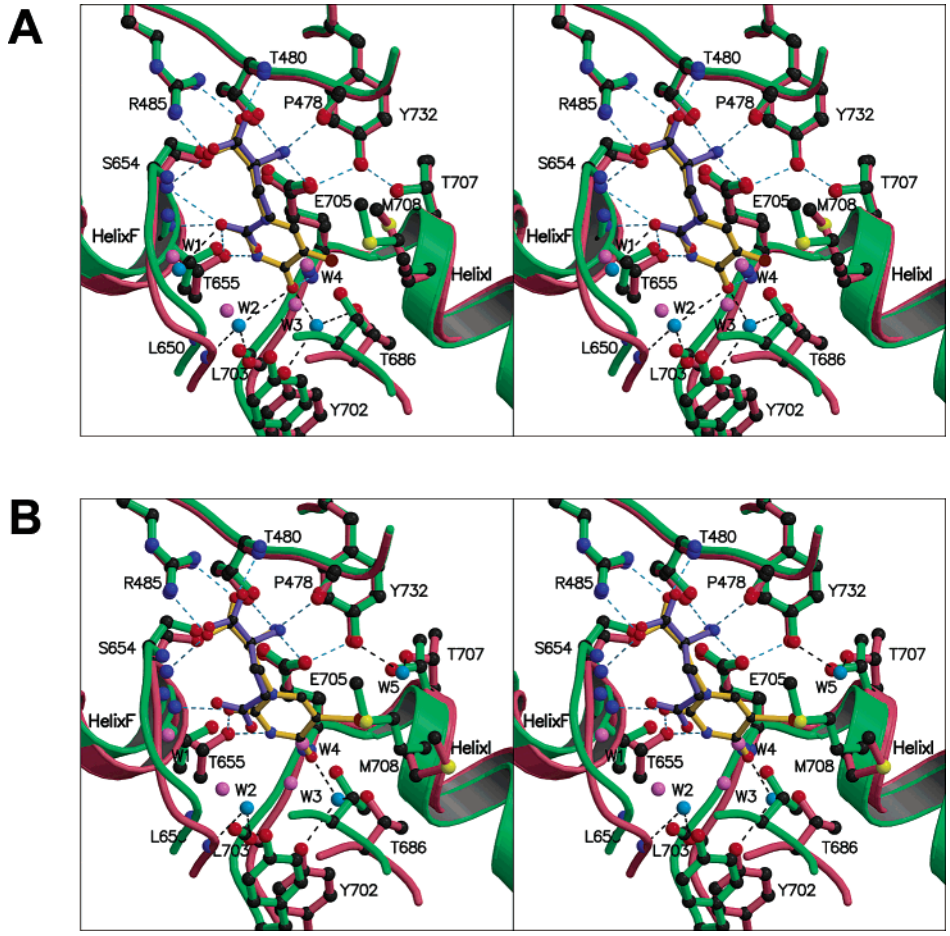

FIGURE 4: The willardiines bind similarly to glutamate but induce a more open cleft conformation in comparison to the glutamate complex. (A) Stereoview of the binding pocket in superimposed FW and glutamate structures. The FW and glutamate complexes are shown in pink and green, while FW and glutamate are yellow and purple, respectively. The ion pair and hydrogen bond interactions between FW and the protein are indicated as dashes; direct interactions to the protein are in cyan, and water mediated interactions are in black. Selected water molecules (W1−4) in the FW and glutamate structures are drawn as cyan and pink spheres, respectively. (B) Stereoview of the binding pocket in superimposed IW and glutamate structures. The glutamate complex is colored as in panel A, and the IW structure is colored the same as FW is colored in panel A. Note that the water W5 is observed in the BrW and IW complexes and not in the HW and FW complexes.

650 and Leu 703, water W2 no longer contributes to subsite E. W2 instead interacts with the 4-carbonyl oxygen atom of HW, FW, and BrW at site F2, making stabilizing ligand−protein interactions (Figures 5 and 6). However, in the IW structure W2 is ~3.8 Å away from the 4-carbonyl oxygen atom of IW and not able to directly interact with any agonist atoms.

5-Substituents of the Willardiines Point to a Partially Hydrophobic Pocket. The 5-methyl group of AMPA and the 5-halogen atoms of the willardiines occupy subsites G and H, respectively. Both subsites are in a partially hydrophobic pocket; subsite G is closer to domain 1, while H is closer to domain 2 (Figure 5). Even though sites G and H are adjacent, their occupancy by agonist atoms has different effects on surrounding residues. The 5-methyl group of AMPA binds at subsite G, and the direct effects are the side chain reorientations of residues Tyr 405 and Met 708. In addition to their effects on Tyr 405 and Met 708, occupancy at site H by a large halogen atom in the BrW or IW structure leads to a significant conformational change of Thr 707, in which the main chain carbon shifts ~1.1 Å (Figure 4). As a consequence, the direct hydrogen bond between Tyr 732 and Thr 707 that is present in the glutamate, quisqualate, AMPA, HW, and FW structures is broken in the BrW and IW complexes. In the latter two structures, the loss of this direct interdomain interaction is compensated by the recruitment of a water molecule (W5) that connects Tyr 732 and Thr 707.

Kainate Occupies Unique Sites in the Ligand-Binding Pocket. Comparison of the full and partial agonist complexes shows that the side chain of Tyr 450 occupies a similar location in all of the structures with the exception of the kainate structure. Although kainate occupies many of the same binding subsites as glutamate (A−F), the isopropenyl group of kainate causes the aromatic ring of Tyr 450 to move approximately 0.8 Å farther into domain 1, as illustrated in Figure 7. On domain 2, Leu 650 does not enter as far into the ligand-binding cleft in comparison to the glutamate complex, for example (*18*). The kainate molecule is also not inserted as deeply into the binding pocket and is located farther from domain 1 in comparison to glutamate, which is also consistent with the more open domain or clam shell conformation of the kainate complex.

In the kainate complex, there is also the loss of two hydrogen bonds between Glu 402−Tyr 450 and Glu 402−Thr 686, as shown in Figure 7. The interaction between Glu 402 and Thr 686 links domain 1 and domain 2. Adjacent to

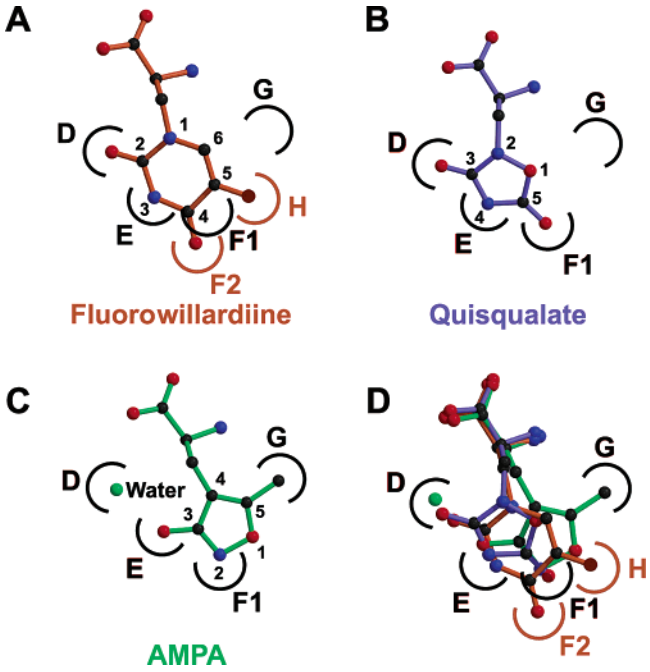

FIGURE 5: Comparison of willardiine and full agonist binding modes. The FW, quisqualate, and AMPA structures are compared after they are superimposed using the main chain α-carbon atoms in domain 1. The conserved binding sites for full agonists (D, E, F1, and G) are labeled in black, while the special binding sites for FW (F2 and H) are shown in orange. (A) The subsite binding regions occupied by the uracil ring of FW; (B) the subsite binding regions occupied by the oxadiazolidine ring of quisqualate (*22*); (C) the subsite binding regions occupied by the isoxazole ring of AMPA and the critical water molecule (*18*); (D) the superimposed structures of all three ligands.

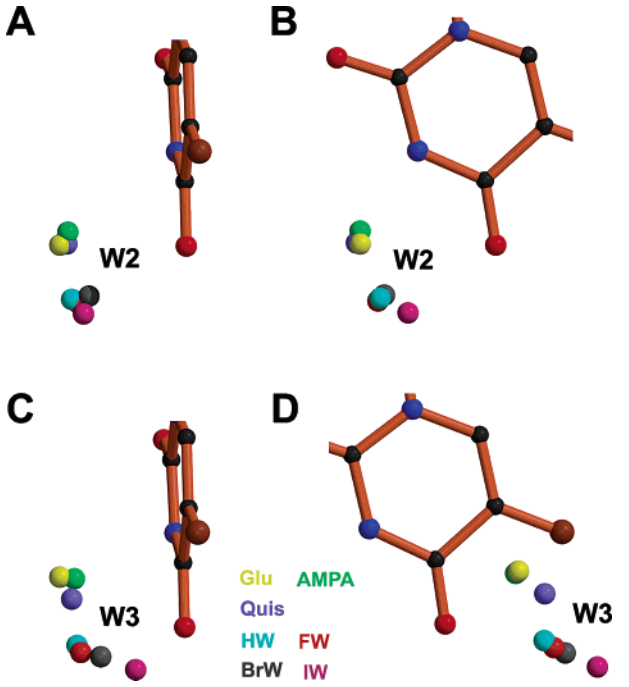

FIGURE 6: Conserved water molecules in the binding pocket (W2 and W3) play critical roles in mediating ligand−protein interactions. Three full agonists (glutamate, quisqualate, and AMPA) and four willardiines (HW, FW, BrW, and IW) are superimposed using the α-carbons from residues in domain 1. W2 is shown in panels A and B, and W3 is shown in panels C and D. For each of them, two views with a ~90° rotation are shown. The water molecules are colored differently according to their parent structures, while only the FW ligand is shown. In panels B and D, ligands are positioned in an orientation similar to what is shown in Figures 4 and 5.

these residues is a conserved hydrogen bond network surrounding the anionic moiety of the agonists involving Arg 485, Tyr 450, and Glu 402 from domain 1, five residues from domain 2 (Thr 686, Tyr 702, Glu 705, Thr 655, and Ser 654), and one water molecule (W3) (Figure 7). This network adjusts to a more open cleft conformation in the willardiine structures. In the IW structure, for example, where the iodine atom at position H induces a significant conformational change of the side chain of Glu 402, a water molecule intercedes and participates in the Tyr 450−water−Glu 402−Thr 686 hydrogen bond interactions. An equivalent water molecule is not present in the kainate structure because it would clash with the kainate isopropenyl group. Kainate thus provides a striking example showing how the occupancy at positions other than the conserved binding sites disrupts presumably favorable interactions in the binding pocket.

Comparison of Packing in Multiple Crystal Forms Reveals Possible Modes of Dimer−Dimer Association. Recent evidence suggests that AMPA receptors are tetramers and are assembled as a dimer-of-dimers (*18*, *27*, *40*−*45*). Inspection of the molecular packing in four different crystal forms reveals patterns of dimer-of-dimer association in which the molecular 2-fold axes of the two adjacent dimers are parallel to each other, and their C termini point in the same direction. We believe that these observations provide a starting point for the studies of dimer−dimer interactions for tetrameric glutamate receptors.

All three full agonists (glutamate, AMPA, and quisqualate) and BrW/IW crystallize in the Zn form, which has three

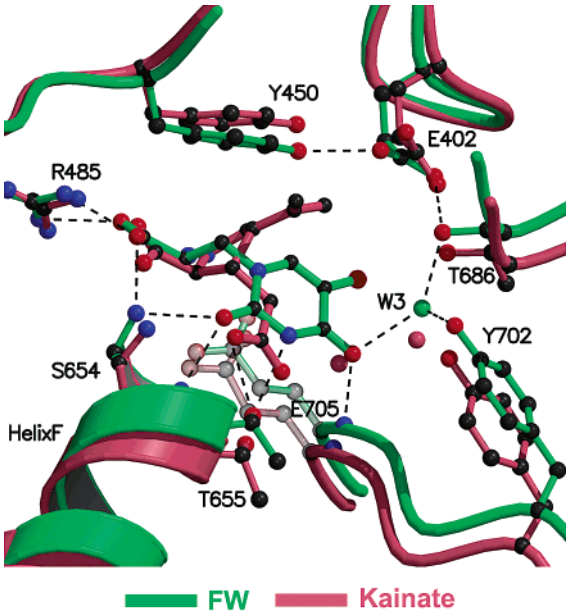

FIGURE 7: Partial agonists, like kainate, that break interdomain interactions lead to open domain conformations and have weaker efficacy than the willardiines. Superimposed kainate and FW structures together with one conserved water molecule (W3) are shown and colored pink and green, respectively. Only the hydrogen bonds in the FW complex are shown and are indicated as dashes.

protomers (A, B, C) in the asymmetric unit (ASU). There are two molecules in the ASU of the quisqualate and IW non-Zn crystal forms, while there is only one molecule in

the ASU of the FW crystal form. The FW crystals are isomorphous to the HW and BrW non-Zn crystal forms. To systematically compare possible modes of dimer−dimer association, we have defined faces on the ligand-binding core protomer as I−IV as illustrated in Figure 8. Face I is the dimer interface. The additional faces are defined as II−IV in a clockwise manner, where the dimer is oriented with the amino terminus closest to the viewer, looking parallel to the molecular 2-fold axis. The dimer interface involves face I and has been discussed in detail (*18*, *27*). Face II is composed of helices A, B, J, and K and loop 1, all of which are contributed by domain 1; face III is made up of residues from both domain 1 and 2; face IV includes helices E−G from domain 2 and loop 2 from domain 1.

Examination of the molecular packing in four different crystal forms reveals that there are three different modes of dimer−dimer association, types A, B, and C. A is the most commonly seen, involves interactions between faces II and IV, and can be divided into three subtypes. Shown in Figures 8A,B and 9 is subtype A1, which is found in the quisqualate non-Zn crystal form and involves 2-fold related interactions between dimers. In the A1 association, the two dimers are positioned side-by-side with face I coplanar. Even though there is no direct interaction between the two dimers as seen in the crystal lattice, a decrease of ∼5 Å in dimer separation along the *X* axis as shown in Figure 8A would lead to II−IV interactions involving loop 1 and helix K of one subunit and helices F and G of another subunit. This mode of potential dimer−dimer interaction has been observed in the structure of GluR2 S1S2J-N754D mutant, in which 511 Å^2 of solvent-accessible surface area per molecule is buried in the interaction (*27*).

The A2 association is similar to A1 and is observed in the Zn form, which also involves a 2-fold related interaction with two I faces parallel to each other (Figure 8C). In this case, there are potential II−II contacts, along with II−IV interactions involving loop 1 and a short loop between helices F and G. The A3 association is found in the IW non-Zn crystal form. In this A3, II−II interaction, loop 1 in one dimer (dimer A) is close to helix K of another dimer (dimer B), and somewhat surprisingly, the side chains of Glu 416 and Asp 769 approach as closely as 3.2 Å. In addition, loop 1 in dimer B is now close to the amino terminus and helix B in dimer A.

The B association involves only III−III interactions where the two ligand-binding pockets are in a face-to-face orientation, as depicted in Figures 8E and F. There are two variations on the B interaction including the B1 subtype in the quisqualate form and the B2 subtype in the HW form. The difference between the B1 and the B2 subtypes is the length of the second translation along the *X* axis. In the B1 interface, the segment between helices G and H in the two neighboring domains define the closest contacts. In the B2 interface, helices G and H in dimer B are close to helix H of dimer A. Type C association is found in the Zn form and involves zinc mediated interactions between face II and face III: a zinc ion interacts with His 435 and Glu 431 from one protomer and Glu 678 from the other protomer, together with a water molecule (Figure 8G). In the C association, the region between helices G and H on face III of dimer B are close to a region on face II of dimer A, which is composed of helices B, J, and K.

DISCUSSION

The application of X-ray crystallography to study conformational changes in proteins and protein−protein interactions is fraught with complexities that primarily arise from the generally unknown and unpredictable effects of interactions between molecules in the crystal lattice. In unfortunate circumstances, lattice interactions can constrain conformational rearrangements and can produce deceptively convincing yet biologically irrelevant protein−protein contacts. Because we are interested in determining the extent to which different agonists stabilize distinct conformational states in the GluR2 S1S2 ligand-binding core and in predicting possible subunit−subunit contacts in the intact receptor, we have determined the extent to which lattice interactions affect the conformational flexibility of the ligand-binding core, and we have studied patterns of subunit−subunit contacts in different crystal forms to predict modes of subunit interactions in the intact receptor.

On the basis of a number of crystallographic investigations, full agonists induce the most closed domain conformation of the GluR2 ligand-binding core (*18*, *19*, *22*), and the willardiine complexes adopt continuously more open conformations in the order of HW < FW < BrW < IW (*29*). Most interestingly, the conformations that the willardiines stabilize are intermediate in domain closure between full agonists, such as glutamate, AMPA, and quisqualate, and the weak partial agonist kainate (*18*, *22*). More specifically, there is a strong correlation between the degree of domain closure and the extents of receptor activation and desensitization, with the extents of activation and desensitization increasing in the order of IW < BrW < FW < HW (*29*). Because the functional behavior of the GluR2 receptor appears to be tightly coupled to the nuances in the conformation of the ligand-binding core, we want to ensure that our crystallographic studies on the S1S2 core are as informative as possible. Therefore, we carried out crystal titration experiments to determine the extent to which the functional and conformational behavior of the GluR2 ligand-binding core is preserved in the crystal. In addition, we have compared the 5-substituted willardiine, glutamate, AMPA, quisqualate, and kainate complexes, together with key water molecules, and we have gained a better understanding of the molecular determinants of partial agonist potency, efficacy, and selectivity. Finally, by taking advantage of different crystal forms, we have analyzed dimer−dimer contacts in the crystal, and we suggest possible modes of dimer−dimer interaction for the ligand-binding core in the intact GluR2 receptor.

Ligand Exchange and Conformational Rearrangement in the Crystal. The structures of the BrW and IW complexes have been determined in two different crystal forms: a Zn form in which five zinc ions mediate interprotomer interactions and a non-Zn form in which there are relatively few protein−protein interactions. Within either crystal form, IW induces less domain closure than BrW. However, the Zn form structures are ∼4° more closed than the non-Zn form structures, showing the substantial perturbation of the structure in the Zn form crystals. By contrast, the full agonist structures solved in Zn and non-Zn forms are almost identical, suggesting that full agonists are able to induce a single, stable conformation. To obviate the effects of strong zinc mediated perturbations of the protein structure, all of

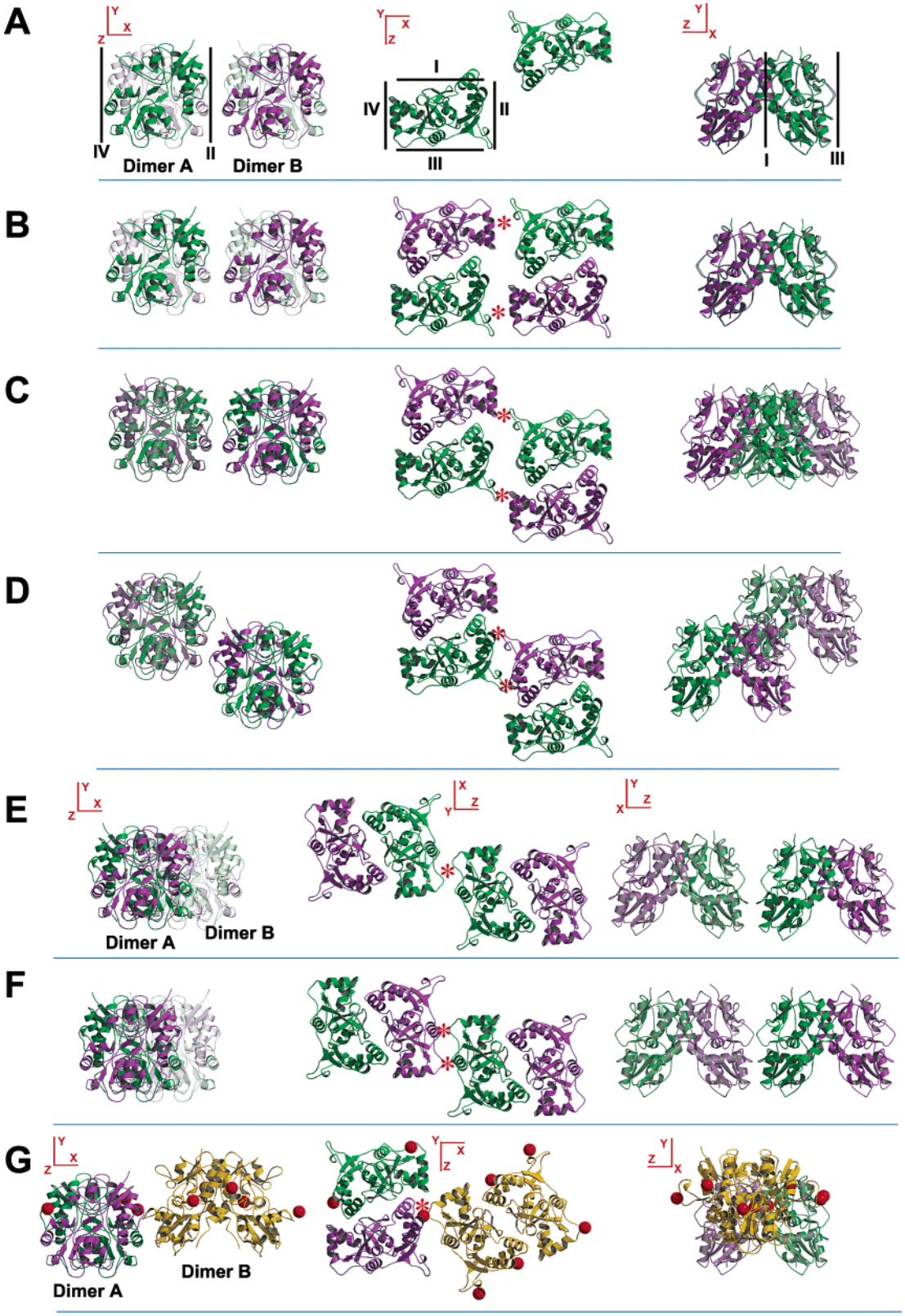

FIGURE 8: Molecular packing in multiple crystal forms reveals possible dimer−dimer interactions of GluR2. The ligand-binding core structures are shown as ribbon diagrams. To simplify structure comparison, a coordinate system is used in which the *Y* axis is parallel to the molecular 2-fold axis, and the *XY* plane is parallel to the dimer interface. All the dimer pairs are viewed from three different orientations, along the *X*, *Y*, and *Z* axes. (A) Four distinct protein surfaces are defined using A1 type dimer pair as an example. In the middle panel, the two purple protomers are omitted to achieve a clear view of a subunit's surfaces, defined as I−IV. Face I is located at the dimer interface. The remaining faces are defined as II−IV, in a clockwise manner, where the amino terminus is closest to the viewer, and the view is parallel to the molecular 2-fold axis; (B) the A1 type dimer pair observed in the quisqualate non-Zn form structure; (C) the A2 type dimer pair observed in the quisqualate Zn form complex; (D) the A3 type dimer pair observed in the IW complex; (E) the B1 type dimer pair seen in the quisqualate non-Zn form structure; (F) the B2 type dimer pair from the HW/FW/BrW complex; (G) the C type dimer pair found in the quisqualate Zn form complex; dimer B is yellow, and the zinc ions are indicated as red spheres. In panels B−G, red stars mark the sites of closest dimer−dimer approach.

the subsequent structure comparisons were carried out using the non-Zn form structures. However, the question still remains: to what extent do studies in crystals reflect the related conformational changes of the ligand-binding core in solution or of the intact receptor in the membrane?

The systematic crystal titration experiments presented in this paper provide direct answers to the questions of ligand-binding affinity and conformational plasticity in GluR2 S1S2 crystals. We show that even with the constraints of the Zn crystal form, the BrW complex adopts a conformation in which the ligand-binding cleft or clam shell is ~2° more open than in the AMPA complex. Furthermore, the competition between AMPA and BrW in crystals leads to a transition between AMPA-like and BrW-like structures, proving that conformational changes can take place in crystals. The EC_{50} value derived from the change in domain closure was 6.8 μM. The competition between ligands in crystals was further explored by directly monitoring the replacement of AMPA by BrW. The occupancy of BrW in the binding pocket was monitored by the amplitude of the bromine peak in anomalous difference Fourier maps, taking advantage of the anomalous scattering of the bromine atom. From these measurements, we obtained an EC_{50} value of 12.9 μM. The crystal titration experiments therefore provide a direct link between agonist binding and protein conformational changes. At the same time, an IC_{50} value of 4.0 μM was obtained from ^{3}H-AMPA displacement experiments with BrW in solution, suggesting that the functional behavior of the GluR2 ligand-binding core in crystals is similar to that in solution. Taken together, these observations indicate that the GluR2 S1S2 ligand-binding core exists in a similar high affinity state in the crystal and in solution. Furthermore, the protein can undergo ligand-induced conformational changes in the crystal, and the lattice interactions do not preclude biologically relevant rearrangements.

Willardiine Potency and Efficacy. The two-electrode voltage clamp (TEVC) dose response experiments, as well as ^{3}H-AMPA displacement studies, showed that the willardiines are highly potent agonists for GluR2 with potency in the order of FW > BrW > IW > HW. FW, for example, has an IC_{50} value of 23.5 nM, which is similar to the IC_{50} of quisqualate (20 nM) (*22*) and the K_D for ^{3}H-AMPA binding (24.8 nM) (*18*). The high potency of willardiines is readily explained by the observation that willardiines bind similarly to full agonists, occupying all the conserved binding sites A−F (Figure 5). Indeed, we had previously suggested that occupying sites D−F would endow an agonist with high potency (*22*). Interestingly, however, the EC_{50} value of FW (0.19 μM) is ca. 5-fold smaller than that of quisqualate (1.2 μM), on the basis of TEVC experiments on the GluR2 receptor under nondesensitizing conditions (*46*). Perhaps one reason the EC_{50} values for quisqualate and FW are so different, yet their binding constants are relatively similar, has to do with the fact that FW is a partial agonist and does not spend as much of its binding energy in gating or opening the ion channel, in comparison to the full agonist quisqualate (*47*).

The willardiines induce a continuously more open cleft conformation in the GluR2 S1S2J ligand-binding core in the order of HW < FW < BrW < IW. Water molecules, acting in concert with variations in the modes of agonist−protein interactions, play a key role in modulating the cleft conformation. Indeed, the willardiines adopt slightly different binding modes in comparison to the full agonists glutamate, quisqualate, and AMPA. For example, in the willardiine complexes, agonist binding site F2 is located ~1.4 Å away from site F1 and is closer to domain 2 (Figure 5), consistent with the more open domain conformation induced by the willardiiines. Agonist atoms in the F1 and F2 subsites interact with the main chain nitrogen atom of Glu 705, a key residue that binds to the α-amino group and undergoes a substantial rearrangement upon agonist binding and domain closure (*18*). Therefore, different positions of sites F1 and F2 might affect domain closure through interactions between the sites and Glu 705. Coupled to subsites F1 and F2 are also the locations of waters W2 and W3. Instead of interacting with full agonists at site E, W2 forms a hydrogen bond with the 4-carbonyl oxygen of HW/FW/BrW at site F2, thus maintaining the interactions between the willardiines and domain 2. The W2−F2 distance increases when BrW and IW are bound and no direct interaction is possible in the IW complex. These differences in local structure might explain, at least in part, the range of potencies within the willardiine family.

The water W3 mediated interactions between sites F1/F2 and Thr 686 and Tyr 702 are maintained in the structures of willardiines, AMPA, glutamate, quisqualate, and kainate complexes as illustrated in Figures 5 and 6. Besides occupying different locations than those in the full agonist complexes, the W3 waters in the willardiine complexes show continuous changes in their positions as shown in Figure 6. In the order of HW, FW, BrW, and IW, W3 moves closer to the dimer interface. In other words, the distance between the two W3 waters in a S1S2 dimer decreases in the order of HW, FW, BrW, and IW, which is consistent with the more open domain conformation and the decrease in linker separation in the HW, FW, BrW, and IW structures (*29*). The relative position of W3 provides a convenient metric that is correlated to the degree of domain closure and linker separation in the full agonist and partial agonist structures.

Even though HW induces the most domain closure and has the greatest efficacy, HW is the least potent willardiine. Indeed, the potencies of the willardiine compounds on GluR2 are correlated to the electronegativity of the 5-substituent, as previously suggested (*15*), because the uracil-like ring of the willardiines must lose a proton to mimic the anionic γ carboxyl group of glutamate. HW has a 5-substituent with the weakest electron withdrawing character, and the pK_a value of HW (9.97) is about 1.21 units higher than that of BrW (8.76) (*48*). The relatively high pK_a value of HW implies that the ionized form is relatively less abundant at physiological pH and thus the apparently high EC_{50} and IC_{50} values may be largely due to a lower concentration of the active, anionic species. In fact, studies on 6-azawillardiine analogues found that the 6-aza substitution resulted in an increase in agonist potency because of the lowering of the pK_a value for the uracil ring (*49*).

Interestingly, the glutamate, AMPA, quisqualate, and willardiine complexes with GluR2 show a similar ligand position in the binding pocket relative to domain 1 and a conserved hydrogen bond network surrounding the γ-substituent, despite the varying cleft conformations (Figure 7). This structural continuity is fostered by residues Tyr 450, Glu 402, and Thr 686, which flank the bound ligand,

constrain its position, and participate in interactions spanning the ligand-binding cleft. To adjust to a partial agonist, such as IW for example, a water molecule is recruited to maintain the Tyr 450−Glu 402 interaction despite the side chain reorientation of Glu 402. In the kainate complex, the Tyr 450−Glu 402−Thr 686 interaction is further perturbed because of an even more open cleft conformation (Figure 7). The importance of this hydrogen bond network is supported by the studies on residue Thr 686 (*50*), which is a threonine in GluR1-4 and KA1-2 and a serine/asparagine in GluR5-7 (*13*, *51*−*53*). Site-directed mutagenesis studies have shown that kainate receptor sensitivity to IW is largely determined by Ser 721 in GluR5 (Thr 686 in GluR2). The OG1 atom of Thr 686 is only 3.7 Å away from the iodine atom in the IW complex. A threonine or serine residue is able to form a hydrogen bond with Glu 402, but an asparagine is too large and the side chain will sterically clash with the iodo substituent on the uracil-like ring. In addition to disrupting the favorable hydrogen bond network, kainate occupies sites D and E in the binding pocket while recruiting a water molecule at site F2, a partial agonist specific binding site. Perturbation of the hydrogen bonding network, along with the other factors discussed previously, contribute to kainate's high IC_{50} (*18*).

Partially Hydrophobic Pocket Modulates Ligand Selectivity. Crystal structures of willardiine complexes show that the 5-halogen atom points to a partially hydrophobic pocket that is surrounded by Glu 402, Tyr 405, Tyr 450, Pro 478, and Tyr 732 from domain 1 and Thr 686, Glu 705, Thr 707, and Met 708 from domain 2. The side chain of Met 708 is located in the middle of this pocket and responds to agonist atoms that bind in this pocket. The willardiine structures clearly show that the side chain reorientation of Met 708 accommodates the 5-halogen atoms. Detailed structure comparisons show that the side chain conformations of Met 708 could be classified into four different states: (1) the glutamate state; (2) the HW/FW/Quis state; (3) the AMPA state; and (4) the BrW/IW state. Met 708 has the greatest freedom to adopt an extended conformation in the presence of glutamate. In comparison with the glutamate state, a rotamer change occurs at Met 708 in the HW/FW/Quis structures and shifts the sulfur atom by ∼1.9 Å (Figure 4).

When agonist atoms bind in the partially hydrophobic pocket, as occurs in the AMPA, BrW, and IW complexes, a substantial reorientation of Met 708 is unavoidable. The sulfur atom of Met 708 moves ∼2.5 Å in the AMPA structure and ∼4.1/4.5 Å in the BrW/IW structures in comparison with the glutamate state. The fact that Met 708 adopts different conformations in the AMPA state and the BrW/IW state suggests that the different locations of the 5-substituents of the willardiines (site H) and the 5-methyl group of AMPA (site G) may have different effects on the receptor structure and function. Interestingly, it is a Ser in GluR5 and a Thr in GluR6/7 at the place of Met 708. The small polar residue at this position probably helps confer unique ligand selectivity to kainate receptors. For example, the potency sequence is IW > BrW > FW > HW for kainate receptors but is FW > BrW > IW > HW for AMPA receptors (*16*, *29*, *49*).

Site G is located in the partially hydrophobic pocket and is surrounded by residues from domain 1. Therefore, binding at site G will mostly affect residues on domain 1 and have little effect on interdomain interactions. Because AMPA is a full agonist, we conclude that occupancy of site G by a methyl group allows for maximal domain closure and receptor activation. In comparison with site G, site H is closer to domain 2 and has a more direct impact on residues on domain 2. The occupancy of site H, with the willardiine complexes as examples, results in partial domain closure and receptor activation. Therefore, site H is an unfavorable binding position for full agonists, and its occupancy distinguishes full and partial agonists. Interestingly, the rupture of the Tyr 732−Thr 707 hydrogen bond in the BrW/IW complexes is compensated by a water molecule (W5). It suggests that the Tyr 732−Thr 707 interdomain interaction is important for stabilizing the closed cleft conformation.

Met 708 and Thr 707 are located at the amino terminus of helix I, and we suggest that the conformational changes at site H might be transmitted to changes in the orientation of helix I. In fact, helix I moves slightly closer to the dimer interface and farther away from the ligand-binding pocket in the willardiine complexes, in comparison with the full agonist structures. In this way, the agonist-induced changes could be relayed by helix I to remote parts of the protein, perhaps via a conserved disulfide bond that connects the carboxyl terminus of helix I (domain 2) and helix K (domain 1).

Possible Modes of Dimer−*Dimer Association*. iGluRs are tetrameric receptors composed of a dimer-of-dimers (*18*, *27*, *40*, *41*). However, there is very little information regarding the nature of the dimer−dimer interactions in the intact receptor. Recently, we have determined the structures of the wild-type GluR2 S1S2J construct in multiple crystal forms and have found that it forms a similar dimer under all conditions, with different dimer−dimer association patterns (Figure 8). The multitude of crystal forms may reveal how dimeric units within an intact, tetrameric receptor interact.

We suggest that the A1 and A2 types represent a starting point for modeling dimer−dimer association modes of the intact receptor, and the A1 type association will be discussed in detail as an example. The other dimer association modes observed are unlikely to be found in intact glutamate receptors because they either lead to dramatically long interdimer distances or the relative positions of the two dimers are too difficult to reconcile with a centrally located, approximately 4-fold rotationally symmetric ion channel.

In the A1 arrangement, the dimer interfaces are coplanar, and the four linker regions, proximal to the transmembrane segments, are in the same plane. With Pro 632 as a marker for the linker, protomers A/D are located at the end of a long diagonal, while protomers B/C are at the end of a short diagonal. The intradimer linker distance is 39 Å, while the interdimer linker distance is 51 Å, the latter of which is the shortest among all observed dimer association modes. A decrease in the interdimer distance by ∼5 Å will lead to II−IV interactions involving loop1/helix K and helix F/G, as already observed in the GluR2-N754D structure (*27*).

However, it is unclear how the A1 association will be reconciled with the probable 4-fold rotational symmetry of the ion channel (i.e., there is a symmetry mismatch between the ligand-binding cores and the ion channel (*27*)). One possibility is that the two dimers will rotate, in opposite directions, around an axis perpendicular to the dimer interface, as illustrated in Figure 9. This movement will tend

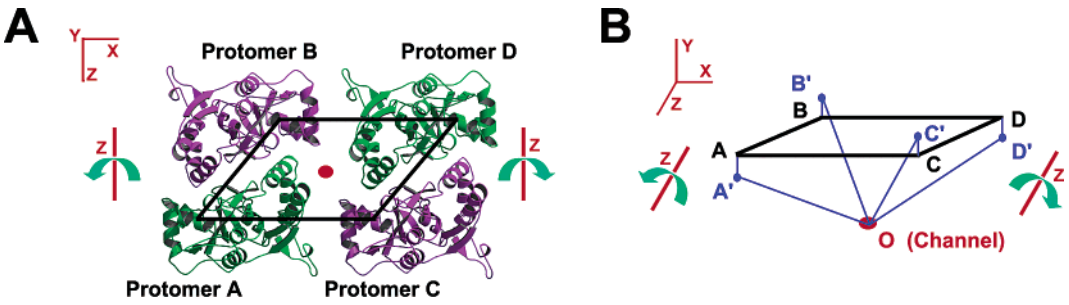

FIGURE 9: Possible mode of dimer−dimer association for the ligand-binding core in intact AMPA receptors based on the A1 dimer-of-dimers. (A) The arrangement of subunits as suggested by the A1 arrangement. The black lines connect residue Pro 632 in each subunit, an amino acid proximal to the linker region and perhaps therefore close to the transmembrane ion channel. The red oval defines the 2-fold axis that relates dimer pair AB to pair CD and may be close to the location of the ion channel. (B) Schematic view of the locations of Pro 632 residues, defined as A, B, C, and D for each of the corresponding subunits, relative to the location of the putative transmembrane region, defined again as a red oval (O). In this arrangement, the distances AO and DO are longer than the distances BO and CO. However, we know that the same polypeptide segments link the ligand-binding cores and the transmembrane domains in all subunits of an AMPA receptor. To equalize the distance between the ligand-binding cores and the transmembrane segments, and to preclude formation of an infinite ribbon of receptors by a simple translation, each AB and CD dimer pair might undergo a rotation, in opposite directions, about the *Z* axis. This will then lead to the new locations of Pro 632 residues of A′, B′, C′, and D′, now making the distances A′O and D′O equal to B′O and C′O. The A1 arrangement of subunits may undergo a rearrangement such as described above in the intact receptor.

to equalize the distance between the linker regions in each of the protomers with the transmembrane channel while minimizing the clash between the two dimers. In this scenario, the four linker regions within a tetramer are no longer coplanar, and the linkers of A and D move closer to the membrane while the linkers of protomers B and C move farther away from the membrane. At some point(s) between the ligand-binding cores and the transmembrane channel, the polypeptide chains will exhibit local asymmetry as required to accommodate the symmetry mismatch. In the arrangement of dimers described above, the flip/flop region at the end of helix K is proximal to the interdimer interface and in a position, perhaps, to modulate the properties of the ion channel (*54*, *55*).

CONCLUSIONS

Here we have employed crystal titration experiments to show that the GluR2 ligand-binding core can undergo conformational changes in the crystal and that its ligand binding properties are similar in the crystal and in solution. Detailed structure comparisons reveal conserved ligand-binding modes of agonists to the GluR2 receptor and define a structural basis for differentiating between full and partial agonists. Possible dimer−dimer arrangements have also been suggested on the basis of dimer−dimer interactions in multiple crystal forms. The structural and functional information presented in this paper support the model that partial agonists induce less domain closure than full agonists and that there is a correlation between the degree of domain closure and the extent of receptor activation and desensitization.

ACKNOWLEDGMENT

Joe Lidestri is acknowledged for management of the X-ray facility at Columbia University, and Craig Ogata is thanked for assistance with data collection at X4A at the National Synchrotron Light Source.

SUPPORTING INFORMATION AVAILABLE

A table of PDB codes associated with the deposited coordinates is provided. This material is available free of charge via the Internet at http://pubs.acs.org.

REFERENCES

1. Dingledine, R., Borges, K., Bowie, D., and Traynelis, S. F. (1999) *Pharmacological Rev. 51*, 7−61.
2. Madden, D. R. (2002) *Nat. Rev. Neurosci. 3*, 91−101.
3. Lees, G. J. (2000) *Drugs 59*, 33−78.
4. Cull-Candy, S., Brickley, S., and Farrant, M. (2001) *Curr. Opin. Neurobiol. 11*, 327−335.
5. Franciosi, S. (2001) *Cell Mol. Life Sci. 58*, 921−930.
6. Lerma, J., Paternain, A. V., Rodriguez-Moreno, A., and Lopez-Garcia, J. C. (2001) *Physiol. Rev. 81*, 971−998.
7. Cavalheiro, E. A., and Olney, J. W. (2001) *Proc. Natl. Acad. Sci. U.S.A. 98*, 5947−5948.
8. Rzeski, W., Turski, L., and Ikonomidou, C. (2001) *Proc. Natl. Acad. Sci. U.S.A. 98*, 6372−6377.
9. Takano, T., Lin, J. H., Arcuino, G., Gao, Q., Yang, J., and Nedergaard, M. (2001) *Nat. Med. 7*, 1010−1015.
10. Bräuner-Osborne, H., Egebjerg, J., Nielsen, E. O., Madsen, U., and Krogsgaard-Larsen, P. (2000) *J. Med. Chem. 43*, 2609−2645.
11. Seeburg, P. H. (1993) *Trends Neurosci. 16*, 359−365.
12. Nakanishi, S., and Masu, M. (1994) *Annu. Rev. Biophys. Biomol. Struct. 23*, 319−348.
13. Hollmann, M., and Heinemann, S. (1994) *Annu. Rev. Neurosci. 17*, 31−108.
14. Chiu, J., DeSalle, R., Lam, H.-M., Meisel, L., and Coruzzi, G. (1999) *Mol. Biol. Evol. 16*, 826−838.
15. Patneau, D. K., Mayer, M. L., Jane, D. E., and Watkins, J. C. (1992) *J. Neurosci. 12*, 595−606.
16. Wong, L. A., Mayer, M. L., Jane, D. E., and Watkins, J. C. (1994) *J. Neurosci. 14*, 3881−3897.
17. Armstrong, N., Sun, Y., Chen, G.-Q., and Gouaux, E. (1998) *Nature 395*, 913−917.
18. Armstrong, N., and Gouaux, E. (2000) *Neuron 28*, 165−181.
19. Hogner, A., Kastrup, J. S., Jin, R., Liljefors, T., Mayer, M. L., Egebjerg, J., Larsen, I. K., and Gouaux, E. (2002) *J. Mol. Biol. 311*, 815−836.
20. Kasper, C., Lunn, M.-C., Liljefors, T., Gouaux, E., Egebjerg, J., and Kastrup, J. S. (2002) *FEBS Lett. 531*, 173−178.
21. Hogner, A., Greenwood, J. R., Liljefors, T., Lunn, M.-C., Egebjerg, J., Larsen, I. K., Gouaux, E., and Kastrup, J. S. (2003) *J. Med. Chem. 46*(2), 214−21.
22. Jin, R., Horning, M., Mayer, M. L., and Gouaux, E. (2002) *Biochem. 41*(52), 15635−15643.
23. Stern-Bach, Y., Bettler, B., Hartley, M., Sheppard, P. O., O'Hara, P. J., and Heinemann, S. F. (1994) *Neuron 13*, 1345−1357.
24. Kuusinen, A., Arvola, M., and Keinänen, K. (1995) *EMBO J. 14*, 6327−6332.
25. Chen, G. Q., and Gouaux, E. (1997) *Proc. Natl. Acad. Sci. U.S.A. 94*, 13431−13436.
26. Chen, G.-Q., Sun, Y., Jin, R., and Gouaux, E. (1998) *Protein Sci. 7*, 2623−2630.
27. Sun, Y., Olson, R. A., Horning, M., Armstrong, N., Mayer, M. L., and Gouaux, E. (2002) *Nature 417*, 245−253.

28. Chen, G.-Q., and Gouaux, E. (2000) *Tetrahedron 56*, 9409−9419.
29. Jin, R., Banke, T. G., Mayer, M. L., Traynelis, S. F., and Gouaux, E. (2003), submitted.
30. Otwinowsky, Z., and Minor, W. (1997) *Methods Enzymol. 276*, 307−326.
31. Brünger, A. T. (1992) *X-PLOR. Version 3.1. A System for X-ray Crystallography and NMR*, Yale University Press, New Haven.
32. Brünger, A. T., Adams, P. D., Clore, G. M., DeLano, W. L., Gros, P., Grosse-Kunstleve, R. W., Jiang, J. S., Kuszewski, J., Nilges, M., Pannu, N. S., Read, R. J., Rice, L. M., Simonson, T., and Warren, G. L. (1998) *Acta Crystallogr. D54*, 905−921.
33. Jones, T. A., Zou, J.-Y., and Cowan, S. W. (1991) *Acta Crystallogr. A47*, 110−119.
34. Brünger, A. T. (1992) *Nature 355*, 472−475.
35. Kleywegt, G. J. (1999) *Acta Crystallogr. D55*, 1878−1884.
36. Lu, G. (2001) http://bioinfo1.mbfys.lu.se/∼guoguang/fit.html.
37. Kraulis, P. J. (1991) *J. Appl. Crystallogr. 24*, 946−950.
38. Esnouf, R. M. (1999) *Acta Crystallogr. D55*, 938−940.
39. Merritt, E. A., and Murphy, M. E. P. (1994) *Acta Crystallogr. D50*, 869−873.
40. Rosenmund, C., Stern-Bach, Y., and Stevens, C. F. (1998) *Science 280*, 1596−1599.
41. Kuusinen, A., Abele, R., Madden, D. R., and Keinänen, K. (1999) *J. Biol. Chem. 41*, 28937−28943.
42. Ayalon, G., and Stern-Bach, Y. (2001) *Neuron 31*, 103−113.
43. Mansour, M., Nagarajan, N., Nehring, R. B., Clements, J. D., and Rosenmund, C. (2001) *Neuron 32*, 841−853.
44. Robert, A., Irizarry, S. N., Hughes, T. E., and Howe, J. R. (2001) *J. Neurosci. 21*, 5574−5586.
45. Bowie, D., and Lange, G. D. (2002) *J. Neurosci. 22*, 3392−3403.
46. Stern-Bach, Y., Russo, S., Neuman, M., and Rosenmund, C. (1998) *Neuron 21*, 907−918.
47. Jones, M. V., Jonas, P., Sahara, Y., and Westbrook, G. L. (2001) *Biophys. J. 81*, 2660−2670.
48. Lidak, M. Y., Dipan, I. V., Paegle, R. A., and Stradyn, Y. P. (1972) *Chem. Heterocycl. Compd. 5*, 644−648.
49. Jane, D. E., Hoo, K., Kamboj, R., Deverill, M., Bleakman, D., and Mandelzys, A. (1997) *J. Med. Chem. 40*, 3645−3650.
50. Swanson, G. T., Green, T., and Heinemann, S. F. (1998) *Mol. Pharmacol. 53*, 942−949.
51. Bettler, B., Boulter, J., Hermans-Borgmeyer, I., O'Shea-Greenfield, A., Deneris, E. S., Moll, C., Borgmeyer, U., Hollmann, M., and Heinemann, S. (1990) *Neuron 5*, 583−595.
52. Egebjerg, J., Bettler, B., Hermans-Borgmeyer, I., and Heinemann, S. (1991) *Nature 351*, 745−748.
53. Bettler, B., Egebjerg, J., Sharma, G., Pecht, G., Hermans-Borgmeyer, I., Moll, C., Stevens, C. F., and Heinemann, S. (1992) *Neuron 8*, 257−265.
54. Sommer, B., Keinänen, K., Verdoorn, T. A., Wisden, W., Burnashev, N., Herb, A., Köhler, M., Takagi, T., Sakmann, B., and Seeburg, P. H. (1990) *Science 249*, 1580−1585.
55. Mosbacher, J., Schoepfer, R., Monyer, H., Burnashev, N., Seeburg, P. H., and Ruppersberg, J. P. (1994) *Science 266*, 1059−1062.

BI020632T